Numerical simulations of light scattering by red blood cells

Karlsson, Anders; He, Jiangping; Swartling, Johannes; Andersson-Engels, Stefan

2003

CODEN:LUTEDX/(TEAT-7116)/1-15/(2003)

Numerical simulations of light scattering by red blood cells

Jiangping He, Anders Karlsson, Johannes Swartling, and Stefan Andersson-Engels

Department of Electroscience
Electromagnetic Theory
Lund Institute of Technology
Sweden

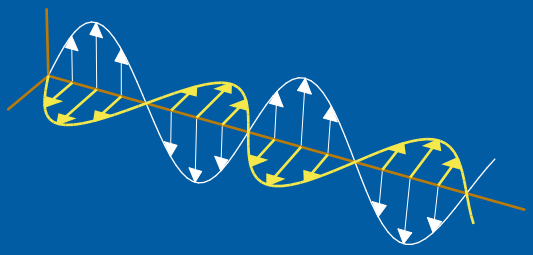

Jiangping He

Department of Electroscience
Electromagnetic Theory
Lund Institute of Technology
P.O. Box 118
SE-221 00 Lund
Sweden

Center for Optical and Electromagnetic Research
Zhejiang university
P.R.China

Anders Karlsson

Department of Electroscience
Electromagnetic Theory
Lund Institute of Technology
P.O. Box 118
SE-221 00 Lund
Sweden

Johannes Swartling

Department of Physics
Lund Institute of Technology
P.O.Box 118
S-221 00 Lund
Sweden

Stefan Andersson-Engels

Department of Physics
Lund Institute of Technology
P.O.Box 118
S-221 00 Lund
Sweden

Editor: Gerhard Kristensson

Abstract

The electromagnetic scattering properties of red blood cells were analyzed by three different methods. The finite-different time-domain method is a general and flexible approach and enables accurate simulations of scattering from objects with arbitrary shape. This method was compared with two approximate methods: the Rytov approximation and the Discrete Dipole Approximation. The interaction of light with a red blood cell was systematically investigated using different wavelengths and orientations of the cells. The simulations show that the cell shape, as well as the cell volume and orientation, have a large influence on the forward scattering.

1 Introduction

Light scattering properties of tissue are important for many medical applications. It governs the light transportation in tissue important for dosimetry of laser therapy [1–3]. Recently, light scattering spectroscopy has attracted much interest [4–6]. Further another biomedical application for which the detailed scattering properties are of great interest is optical analysis of blood. Blood analysis are useful diagnostics tools for many blood related diseases. Among these analysis, optical measurement on blood, both *in vivo* and *in vitro*, is a growing field, since useful information can be extracted with rather simple and nondestructive measurement procedures. A good understanding of the interaction of light with blood is a prerequisite for optical blood analysis. Blood optics is special in several ways, motivating special efforts in improving the understanding of light transportation in blood. Light is heavily scattered by non-spherical red blood cells (RBCs), not containing any scattering internal structures. Alignment and aggregation of RBCs are also known to alter light propagation through blood [7].

It is known that the scattering and absorption of light in blood are largely governed by the red blood cells. It is the refractive index of RBCs, as well as their size, shape and orientation, that determine how light propagates. Until recently it has been impossible to perform very accurate simulations of scattering of light from RBC, due to limitations in computer speed and memory. The size of an RBC is typically 5-10 wavelengths in the optical region and the full wave methods require fast computers with large RAM, when applied to such large objects. The contrast between the blood cell and the surrounding plasma is quite small. At a vacuum wavelength of 630 nm the typical values for the index of refraction is 1.40 for a blood cell and 1.35 for the plasma. Thus the blood cell is a weakly scattering object and it is anticipated that approximate methods are applicable. In the paper the accurate calculations by a finite-difference time-domain (FDTD) method are compared with the calculations from two approximate methods: the Rytov approximation and the discrete dipole approximation (DDA) method. The results obtained with the approximate methods agree surprisingly well for a realistic RBC model. A third approximation, referred to as the superposition approximation, is also investigated in the paper.

In the paper, several numerical methods are applied to model light scattering of a single RBC. Calculations are performed for different wavelengths and incident angles to better understand the influence of the shape on the scattered field. It is well known that RBCs, *in vivo* or *in vitro*, display a number of different shapes [8]. In general, the normal RBC shape is a discocyte, i.e. an axially symmetric disk, slightly indented on the axis and having the mirror plane symmetry perpendicular to the axis. The information from these calculations are useful in the development of models of light propagation in whole blood containing many RBCs. Scattering of the light from realistic RBC shapes (*i.e.*, disk-like shpae) is also investigated.

The FDTD approach is general and flexible and was recently applied to biological scattering problems: [9, **?**]. It enables the simulation of scattering from inhomogeneous objects of arbitrary shape. Today it is one of the best full wave method for accurate simulations of the scattering of light from a small number of blood cells. Several other full wave methods, such as Mie theory, anomalous diffraction approximations [11], multiple solution [12], T-matrix methods [7], have been utilized to study the light scattering from biological cells. Each of these methods has advantages but are limited by geometric assumptions. Section 3 contains a short description of some of these methods, as well as more detailed descriptions of the FDTD method, the Rytov approximation, and the DDA method. The numerical results are collected in Section 4 and in Section 5 some concluding remarks and comments on future work are given.

2 Preliminaries

In the simulations the refractive index for the RBC is set to $n_1 = 1.406$ and the refractive index of the surrounding blood plasma is set to $n_2 = 1.345$. The absorption is neglected in both regions. The model of the disk-like normal RBC used in the simulations is defined in the references [13, 14] with a volume of the RBC of 94 μm^3. The membrane of RBCs has a negligible influence on the scattered field, *cf.* [15, 16] and hence the RBC models do not include the membrane or any other internal structure. Figure 1 shows the cross section of the disk-like RBC model, where the enclosing box has height $a = 2.547\mu$m and length $b = 7.76\mu$m. The three-dimensional (3D) shape is obtained by rotating the cross section around the z axis. Figure 2 depicts the 3D picture of the disk-like RBC model. In the simulations, the incident wave is a time-harmonic linearly polarized plane wave. It propagates in the positive z-direction with the electric field in the x-direction. With the time convention $e^{-i\omega t}$, the complex incident electric field is given by

$$\boldsymbol{E}_{\text{inc}}(z) = \hat{x} E_0 e^{ikz}, \tag{2.1}$$

where $k = n_2\omega/c_0$ is the wave number for the plasma and c_0 is the velocity of light in vacuum. The RBC is rotated around the $y-$direction in order to change the angle of incidence. The rotation angle of the axis of symmetry relative the z-direction is denoted θ_i. Figure 1 shows the case when $\theta_i = 0^\circ$ degrees. To interrelate the angular distributions of the scattered light of different incident wavelengths and angles, the

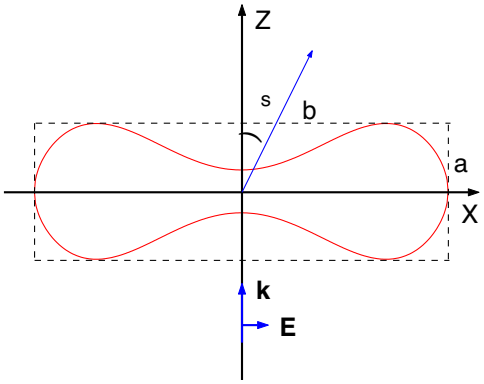

Figure 1: RBC cross section

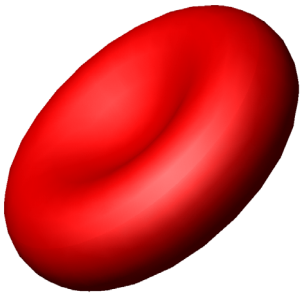

Figure 2: 3D RBC

scattering probability was calculated as a function of the zenith scattering angle θ_s (*cf.* figure 1) This scattering probability, $P(\theta_s)$, was calculated by numerical integration of the differential scattering cross section, $\sigma_{\text{diff}}(\theta_s, \phi_s)$, over all azimuthal angles $\phi_s \in [0, 2\pi]$:

$$P(\theta_s) = \frac{\int_0^{2\pi} \sigma_{\text{diff}}(\theta_s, \phi) \sin\theta_s d\phi}{\int_0^{2\pi}\int_0^{\pi} \sigma_{\text{diff}}(\theta, \phi) \sin\theta d\theta d\phi}. \tag{2.2}$$

The differential cross section is defined by

$$\sigma_{\text{diff}}(\theta, \phi) = r^2 \frac{< \boldsymbol{S}(r, \theta, \phi) \cdot \hat{r} >}{< \boldsymbol{S}_{\text{inc}} \cdot \hat{z} >}$$

where

$$< \boldsymbol{S}_s(r, \theta, \phi) >= \frac{1}{2}\text{Re}\{\boldsymbol{E}(r, \theta, \phi) \times \boldsymbol{H}^*(r, \theta, \phi)\}$$
$$< \boldsymbol{S}_{\text{inc}} >= \frac{1}{2}\text{Re}\{\boldsymbol{E}_{\text{inc}}(z) \times \boldsymbol{H}^*_{\text{inc}}(z)\} = \frac{1}{2}\frac{n_2}{\eta_0}|E_0|^2\hat{z}$$

are the time averages of the Poynting vector of the scattered and incident fields, respectively. Furthermore, $\hat{r}$ is the radial unit vector, $\boldsymbol{E}(r, \theta, \phi)$ is the scattered electric field, $\boldsymbol{H}^*(r, \theta, \phi)$ is the complex conjugate of the corresponding magnetic field and $\eta_0 = 120\pi\Omega$ is the wave impedance of vacuum. Unless otherwise is specified, the wavelengths in the paper are the values in vacuum.

3 Methods

In this section some of the methods that are applicable to the RBC problem are described briefly. The index of refraction of the blood cell is almost the same as that of the surrounding plasma and hence the multiple scattering effects in the blood cell are small. This suggests that approximate methods are applicable. This section discusses three different approximate methods: the superposition approximation, the Rytov approximation, and the DDA method.

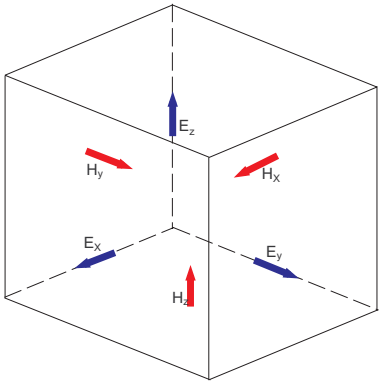

Figure 3: Unit cell in 3D FDTD algorithm

3.1 FDTD: Yee's Method

The FDTD algorithm was originally proposed by K. S. Yee in 1966 [17]. Readers interested in FDTD are recommended the book by Taflove [9], which gives a good overview. The FDTD algorithm numerically solves the Maxwell's curl equations in time domain. In the 3D case, the Maxwell's curl equations are discretized in time and space, resulting in six coupled scalar finite-difference equations in Cartesian coordinates. All three electric field components and all three magnetic components are spatially allocated as in figure 3. The electric and magnetic fields are temporally offset and stepped in a leap frog scheme using the finite-difference form of the curl operator. In order to get the angular far-field distribution of the scattered light, several techniques are required:

1. **Absorbing boundary condition (ABC)** Because of the finite computational domain, the values of the fields on the boundaries must be defined so that the solution region appears to extend infinitely in all directions. With no truncation conditions, the scattered waves will be artificially reflected at the boundaries leading to inaccurate results. The perfectly matched layer (PML) ABC suggested by Berenger [18] have been implemented in the three-dimensional FDTD program and is used in the examples in the paper.

2. **Total field/scattered field** Since this work considers the scattering patterns, the total field/scattered field formulation is used. The computational grid is divided into two regions. The total field region encloses the scatterers whereas the scattered field region, where only the scattered field components are stored, encloses the total field region, as illustrated in Figure 4. At the border between the two regions, special connecting conditions are required, where the incident field is either added or subtracted from the total field. The conditions used for the simulations in the paper are described in detail in Ref [9].

3. **Far-Field Transformation** The FDTD is inherently a near-field method. To determine the far-field scattering pattern, the near-field data is transformed to the far-field by the near-field to far-field (NFFF) transformation. The details of the NFFF technique can be found in [9].

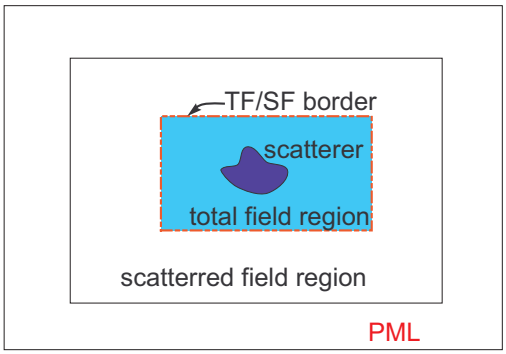

Figure 4: Total field/scattered field regions

3.2 The T-matrix method

This method was originally developed by Waterman [19]. It is also referred to as the null-field method. The method is based on the surface integral representation of the electric field and on expansions of the surface fields in sets of vector functions that are complete on the unit sphere. The incident, reflected, and internal fields are expanded in vector wave functions. From the boundary conditions it is possible to derive a relation between the expansion coefficients of the scattered and of the incident fields. The coefficients are related by a matrix referred to as the T-matrix. The method is very efficient for objects that are less than a few wavelengths in diameter. It converges also for larger objects but then the size of the matrix increases and cancellation effects become significant. In [7] the T-matrix was applied to the scattering from blood cells in the shape of oblate spheroids. A modified version of a computer program developed by Barber et al [20] was used for these calculations. In order to get an acceptable accuracy it was necessary to use quadruple precision, *i.e.*, real numbers with 32 digits precision. It was not possible to obtain accurate results for blood cells with realistic shape. It seems that the T-matrix method has to be pushed to its limits in order to give accurate results for blood cells. However, when it can be applied it is faster than *e.g.*, FDTD.

3.3 Mie scattering

Mie scattering is restricted to scattering from spheres. The known incident field and the unknown internal field are expanded in regular vector waves. The unknown scattered field is expanded in outgoing vector waves. The relation between the expansion coefficients for the incident and scattered fields are derived from the boundary conditions at the surface of the sphere. The relation is given by a diagonal matrix. The matrix is the T-matrix for the sphere and it can also be derived from the T-matrix method. Since the T-matrix is diagonal one does not get the same numerical problems that occurs for non-spherical objects. It is possible to get accurate numerical results also for very large spheres, and the calculations are very fast. Mie scattering is often used as a reference method for other numerical methods.

3.4 The Method of Moments (MoM)

The MoM is a full wave method that is used for the solution of the volume integral equations that can be derived from the Maxwell equations. There are a number of different techniques to speed up the convergence of the method [21]. The method can be applied to the scattering from blood cells but it has not been tested in the paper.

3.5 The Discrete Dipole Approximation

The Discrete Dipole Approximation (DDA) is closely related to the method of moments. The original derivation of the method does not rely on the volume integral equation. Instead it is derived in a less rigorous manner. The principle of the method is as follows: The scattering volume is divided into N parts. Each part is small enough to be represented by a dipole moment. Linearity of the medium implies that the induced dipole moment of each volume element is equal to the electric field in the volume multiplied by the polarizability of the volume. The electric field is a superposition of the fields from the sources external to the object and the electric fields from the sources inside the object, in this case the N dipoles. The field from the external sources is the incident plane wave and hence the electric field in volume j is given by

$$\boldsymbol{E}(\boldsymbol{r}_j) = \boldsymbol{E}_{\text{inc}}(\boldsymbol{r}_j) + \sum_{k \neq j} \mathbf{A}(\boldsymbol{r}_j, \boldsymbol{r}_k) \cdot \boldsymbol{p}(\boldsymbol{r}_k) \tag{3.1}$$

The term $\mathbf{A}(\boldsymbol{r}_j, \boldsymbol{r}_k) \cdot \boldsymbol{p}(\boldsymbol{r}_k)$,where $\mathbf{A}(\boldsymbol{r}_j, \boldsymbol{r}_k)$ is the Green dyadic, is the electric field at a position $\boldsymbol{r}_j$ from a dipole at position $\boldsymbol{r}_k$. It can be found in basic textbooks in electromagnetic theory. The equation is usually not solved by direct inversion. Instead the conjugate gradient method is applied. A more detailed description of the method is given by [22, 23]. In figure 5, the scattering probabilities for a disk-like RBC using FDTD and DDA method are showed. The scattering probabilities agrees very well.

3.6 Superposition

The superposition approximation is based on the assumption that multiple scattering effects are small within the cell. The scattering object is divided into several parts. Each part is viewed as a scattering object and the multiple scattering effects between the objects are neglected. The advantage is that the volume of the scattering object is reduced. That implies a reduction of the CPU-time and the required RAM of the computer. In the example a blood cell was divided in two halves through the yz-plane. The far-field pattern $\boldsymbol{E}_\phi$ in yz-plane for each half was calculated by the FDTD method. Then the two far-fields were added and compared with the same far-field from the whole blood cell. The patterns agree very well, as seen from Figure 6. The superposition approximation facilitates the calculation of far-fields from very large, weakly scattering, objects.

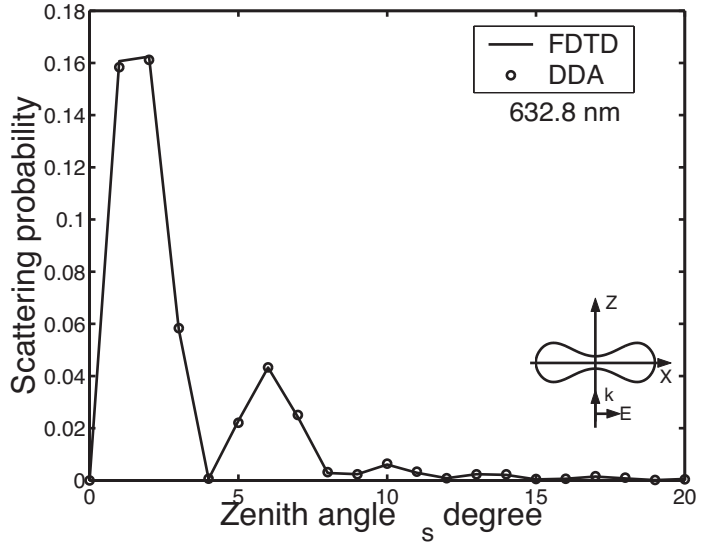

Figure 5: The scattering probabilities for a disk-like RBC using FDTD and DDA method. ($\theta_i = 0°, \lambda = 632.8\,\text{nm}$)

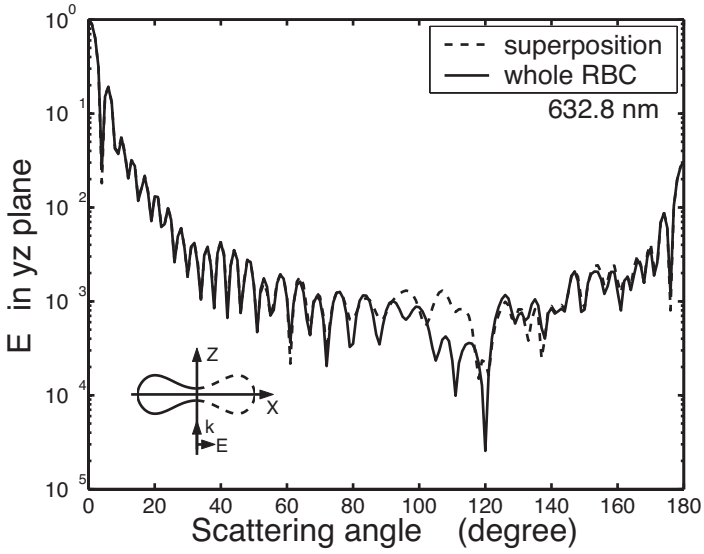

Figure 6: The normalized simulation result of scattered field $\boldsymbol{E}_\phi$ in the yz-plane using FDTD. The solid line is for the whole RBC. The dash line is the superposition of the scattered for field from the left and right halves of the whole RBC. ($\theta_i = 0°, \lambda = 632.8\,\text{nm}$)

3.7 The Rytov approximation

The Rytov approximation is a frequently used method in tomography, [24, 25]. It is then utilized for the inverse scattering problem of determining the permittivity or conductivity of an object. In the paper it is applied in its simplest form to the scattering of a plane wave from an object in a homogeneous lossless medium. The method can be explained as follows: Consider an object that occupies the volume V. Let the index of refraction be n_1 for the object and n_2 for the surrounding medium. The incident wave is given by Eq. (2.1). The approximation assumes that when the wave passes the object, the phase of the wave is shifted while its amplitude and polarization are unaltered. The wave is assumed to travel as straight rays parallel to the z-axis, *i.e.*, along lines $\boldsymbol{r} = (x, y)$. Let $d(x, y)$ be the total distance the ray travels inside the scattering object. If $z = z_1$ is a plane behind the object, the total electric field in that plane reads

$$\boldsymbol{E}(x, y, z_1) = \hat{x} E_0 e^{ik_0(n_2 z_1 + (n_1 - n_2)d(x,y))}$$

Thus the phase is shifted an angle $k_0(n_1 - n_2)d(x, y)$ compared to the incident wave. The far-field amplitude is given by the near-field to far-field transformation, *cf.* [9], *i.e.*,

$$\boldsymbol{F}(\theta, \phi) = i\frac{k^2}{4\pi} E_0 e^{ikz_1} \hat{r} \times \iint_S (\hat{y} - \hat{r} \times \hat{x}))\, (e^{ik_0(n_1 - n_2)d(x,y)} - 1) e^{-ik\hat{r}\cdot\boldsymbol{r}} \mathrm{d}x\mathrm{d}y$$

where S is the plane $z = z_1$. Notice that the integrand is zero outside the projection of the blood cell on the plane $z = z_1$. All reflections of the wave are neglected. Consequently, the approximation gives a far-field amplitude that is only accurate for angles $\theta < \pi/2$. Despite these approximations the calculated far-field pattern is quite accurate, as can be seen in Figure 7. The code for the far-field amplitude is very short and simple and hence the method is an alternative to the far more time and memory requiring full wave methods, *e.g.*, FDTD.

The Rytov approximation can be more accurate. In that case the internal field inside the scattering object is approximated by an inhomogeneous plane wave with constant amplitude but with a phase that varies in the xy-planes. The phase function is then approximately given by a Green function to the Helmholtz equation. This more accurate approximation has not been tested here, but it is anticipated that it gives somewhat better results than the current method.

3.8 The Born approximation

The Born approximation [26] is the solution obtained by the first order iteration of an integral equations for scattering problems, *i.e.*, , the first term in the Neumann series solution to the integral equation. The basic principle is that the induced polarization inside the scattering object is approximated by the incident wave multiplied by the susceptibility function. It is obtained from the DDA method by neglecting the item $\sum_{k \neq j} \mathbf{A}(\boldsymbol{r}_j, \boldsymbol{r}_k) \cdot \boldsymbol{p}(\boldsymbol{r}_k)$ in equation (3.1). The method is limited by the size of the

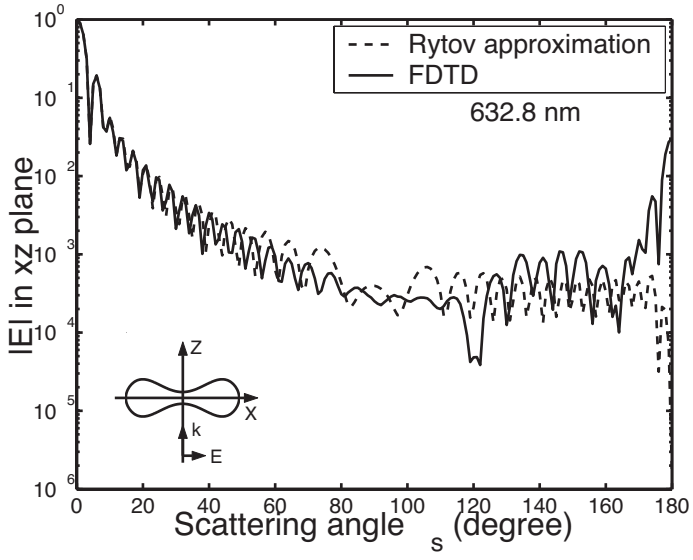

Figure 7: The normalized simulation results of the scattered field $|\boldsymbol{E}|$ in the xz-plane by a disk-like RBC using Rytov approximation and FDTD. ($\theta_i = 0°, \lambda = 632.8\,\text{nm}$)

object. A blood cell is too large in the optical regime for the Born approximation to be valid. The Born approximation was tested but did not give results that were accurate enough.

4 Results and discussions

The simulations show that the FDTD method and the DDA method are both very accurate for scattering from one RBC. The more approximate methods are almost as good as FDTD. Since they are very easy to implement on a computer, they are useful tools that can be used to verify results from other methods. In the rest of the paper only the FDTD method has been used since it is the most robust method.

In this section the scattering properties of the RBC are investigated by the FDTD method. The simulation program *SEMCAD* [27] was used for the simulations of the far-field scattering pattern. In all the FDTD simulation cases, the grid space was adaptively set between $\lambda/10$ and $\lambda/20$ in order to yield accurate results.

4.1 Influence of the shape

It is interesting to understand the effect the shape of the RBC has on the scattering properties. For this reason, scattering patterns were calculated for volume-equivalent RBCs with the oblate spheroidal shape and with the disk-like shape. The same material parameters were used for the two cases. The (vacuum) wavelength was 632.8 nm and the incident angle θ_i was 0° degree. Figure 8 shows the small- angle scattering patterns. It is clear that in the angular interval $\theta_s \in [0°, 8°]$ the disk-like RBC has a much more pronounced second scattering peak than the oblate RBC.

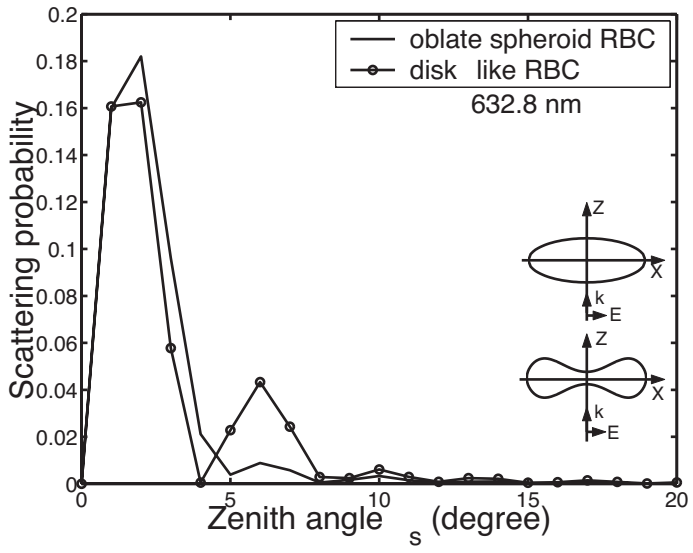

Figure 8: The scattering probabilities for an oblate spheroid with semi-axes 1.47 μm and 3.91 μm, and a disk-like RBC with the same volume. ($\theta_i = 0°, \lambda = 632.8\,\text{nm}$)

This shows that the shape of the RBC has a significant influence on the angular distribution of the scattered light.

4.2 The influence of incident wavelengths and incident angles

To investigate the dependence of the incident wavelengths and incident angles on a disk-like RBC, systematic and accurate simulations were conducted by the FDTD method. Three cases were simulated. The incident angles θ_i for three cases were 0°, 45°, 90° degrees, respectively. For each of the cases the two incident wavelengths 600 nm to 1000 nm were used.

4.2.1 $\theta_i = 0°$ case

Figure 9 demonstrates that the incident wavelengths have a strong influence on the scattering pattern for $\theta_i = 0$. It is seen that the small-angle scattering patterns have two main peaks. The first peak is much larger than the second peak for each wavelength. When the wavelength increases, the first peak expands. The intensity of the peak decreases, but the location of the peak does not change much. The second peak moves towards larger angles when the wavelength increases. The second peak also expands and the intensity of the peak decreases as the wavelength increases. It is well known by scattering theory that the width of the forward peak, θ_f, is approximately proportional to the ratio of the wavelength λ to the particle size a, when the particle is large compared to the incident wavelength:

$$\theta_f \sim \frac{\lambda}{a}. \tag{4.1}$$

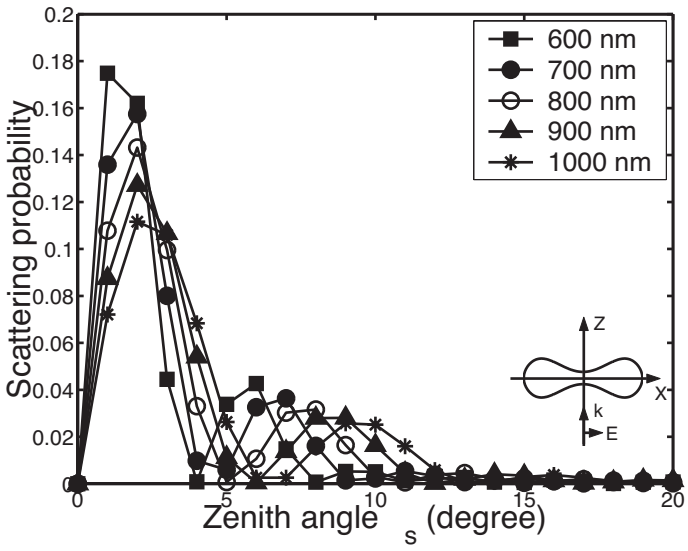

Figure 9: The scattering probabilities for a disc-like RBC excited by incident plane waves with five different wavelengths. The angle of incidence is $\theta_i = 0°$.

The conclusion of (4.1) is useful in the interpretation of the simulations. The increase of wavelength gives the same result as a decrease of the size of the RBC.

4.2.2 $\theta_i = 45°$ case

The same simulations as in the previous case were conducted for the case $\theta_i = 45°$. It is interesting to compare the 45° degree case with the 0° degree case. The scattering pattern of the first peak in the 45° degree case did not change much relative to the 0° degree case, for each wavelength. However, the second peak is much less pronounced.

4.2.3 $\theta_i = 90°$ case

The scattering patterns for $\theta_i = 90$ differ from the two cases above. The scattering patterns are quite insensitive to a change of the wavelengths. The main peaks are much broader and the amplitudes are only half of that in the cases 1 and 2. The geometrical cross section is much smaller than in case 1 and 2. This makes the scattering patterns of each wavelength more uniform. Compared with case 1, the optical thickness is larger. This may result in lower intensity of the forward scattering patterns.

5 Conclusions

Traditionally, light propagation in biological tissues has primarily been modeled by means of radiative transport theory, which takes on a macroscopic view of the scattering properties of the medium. However, in certain cases the microstructure

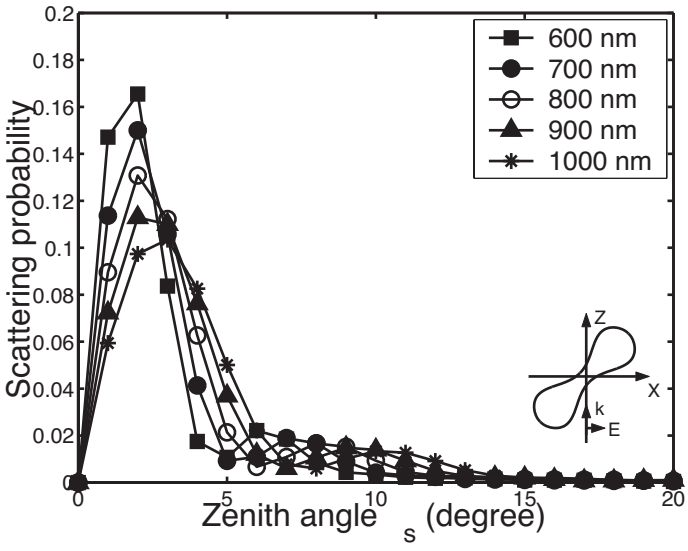

Figure 10: The same cases as in Figures 9 and 11 but for an incident angle of $\theta_i = 45°$ degree

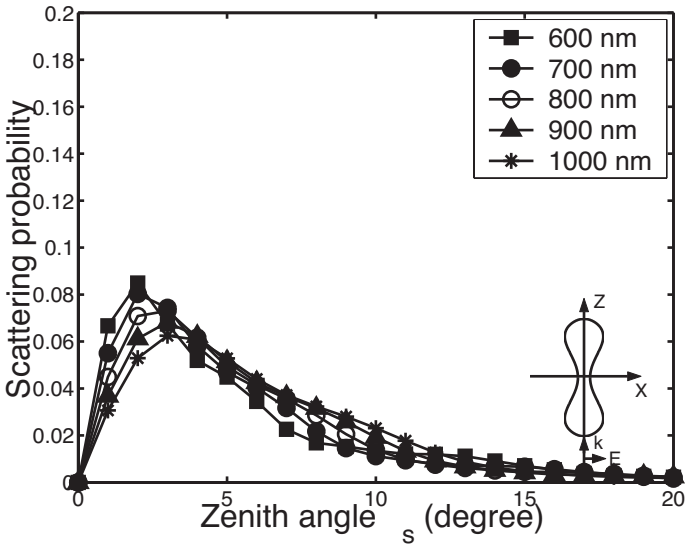

Figure 11: the same cases as in Figures 9 and 10 but for an incident angle of $\theta_i = 90°$ degree

of the medium must be considered, calling for wave solution methods to solve the scattering problem. An example is elastic scattering spectroscopy, which seeks to relate the experimentally measured scattering spectrum to the shape and density of the microscopic scattering centers - the cellular structure - in the tissue.

Optical blood analysis is another area where detailed solutions to the scattering problem are necessary to describe the light interaction with the medium. In this work we have investigated methods to determine the scattering from RBCs that previously have attracted little or none interest for this particular problem. The potential advantages with these methods over previous approaches - most notably, Mie and T-matrix methods - are that they make it possible to use very realistic shapes of the cells, and also that they are not in principle limited to single scatterers.

The general and flexible numerical approach FDTD (the finite difference time domain method) was employed to study the scattering properties of RBCs with a realistic shapes. The difference between the far-field patterns for the RBC with realistic shape and the oblate spheroidal shape emphasizes that it is important to use a realistic shape in order to extract the scattering properties of the RBC. In particular, the spherical models of RBCs used in Mie scattering are not accurate enough. This is further confirmed by simulations that show that the far-field patterns depend strongly on the incident angle (i.e. the orientation of the RBC). The strong dependence on the orientation of the RBCs implies that light propagation in blood in motion differs from that in stationary blood, since the RBCs in flowing blood tend to align along a preferred direction. The incident wavelength has a significant influence on the angular distribution of scattered light; especially when the angle between the incident wave vector and the RBC symmetry axis is small.

Two approximate methods were tested numerically in the paper. Due to the low contrast between the RBC and the plasma, the multiple reflections are weak. For this reason the approximate methods give very good results.

In this work we have demonstrated the usefulness of FDTD and the approximate methods to describe the scattering from single RBCs. Furthermore, the methods have been compared with and validated against previous methods, such as Mie theory and T-matrix theory. As stated above, one of the principal advantages with the methods described in this work are the potential for modeling multiple scattering effects from many closely spaced cells. Such effects have been shown to have decided significance for the scattering from whole blood, and simpler methods such as Mie theory fail to make accurate predictions of this case. In a coming paper, scattering from multiple blood cells are investigated by the FDTD method and by approximate methods. The cross-polarization effects are also analyzed in more detail.

Acknowledgment

We wish to acknowledge the Swedish Research Council for their financial support of this project.

References

[1] T. Johansson, M. Soto Thompson, M. Stenberg, C.af Klinteberg, S. Andersson-Engels, S. Svanberg and K. Svanberg, "Feasibility study of a novel system for combined light dosimetry and interstitial photodynamic treatment of massive tumors," *Appl. Opt.* vol. 41, pp. 1462–1468, 2002.

[2] S. Iinuma, K. T. Schomacker, G. Wagnieres, M. Rajadhyaksha, M. Bamberg, T. Momma and T. Hasan, "In vivo fluence rate and fractionation effects on tumor response and photobleaching: photodynamic therapy with two photosensitizers in an orthotopic rat tumor model," *Cancer Res JID - 2984705R* vol. 59, pp. 6164–6170, 1999.

[3] L. Lilge, K. Molpus, T. Hasan and B. C. Wilson, "Light dosimetry for intraperitoneal photodynamic therapy in a murine xenograft model of human epithelial ovarian carcinoma," *Photochem Photobiol JID - 0376425* vol. 68, pp. 281–288, 1998.

[4] I. J. Bigio, S. G. Bown, G. Briggs, C. Kelley, S. Lakhani, D. Pickard, P. M. Ripley, I. G. Rose and C. Saunders, "Diagnosis of breast cancer using elastic-scattering spectroscopy: preliminary clinical results," *J Biomed. Opt.* vol. 5, pp. 221–228, 2000.

[5] I. J. Bigio, J. R. Mourant and G. Los, "Noninvasive, in-situ measurement of drug concentrations in tissue using optical spectroscopy," *J Gravit. Physiol* vol. 6, pp. 173–175 1999.

[6] J. R. Mourant, T. M. Johnson, G. Los and I. J. Bigio, "Non-invasive measurement of chemotherapy drug concentrations in tissue: preliminary demonstrations of in vivo measurements," *Phys. Med. Biol.* vol. 44, pp. 1397–1417, 1999.

[7] Annika M. K. Nilsson, Peter Alsholm, Anders Karlsson, Stefan Andersson-Engels, "T-matrix computations of light scattering by red blood cells," *Applied Optics*, vol. 37, no. 13, pp. 2735–2748, May 1998.

[8] M. Bessis, "Red cell shapes: An illustrated classification and its rationale," *Nouv. Rev. Fr. Hematol.*, vol. 12, pp. 721–746, 1972.

[9] A. Taflove, *Computational Electrodynamics: The Finite Different Time Domain Method*. Boston: Artech, 1995.

[10] Rebekah Drezek, Andrew Dunn and R. Richard-Kortum, "Light scattering from cells: finite-different time-domain simulations and goniometric measurements," *Applied Optics*, vol. 38, no. 16, pp. 3651–3661, June 1999.

[11] G. J. Streekstra, A. G. Hoekstra, E.-J. Nijhof and R. M. Heethaar, "Light scattering by red blood cells in ektacytometry: Fraunhofer versus anomalous diffraction," *Applied Optics*, vol. 32, pp. 2266–2272, 1993.

[12] G. Videen and D. Ngo, "Light scattering multiple solution for a cell," *J. Biomed. Opt.*, vol. 3, pp. 212–220, 1998.

[13] E. Evans and Y. Fung, "Improved measurement of the erythrocyte geometry," *Microvascular research*, vol. 4, pp. 335–347, 1972.

[14] P. Alsholm, "Light scattering by individual and groups of spheroidal particles," Lund report on atomic physics, Lund Institute of Technology, Tech. Rep. LRAP-200, August 1996.

[15] R. A. Meyer, "Light scattering from red blood cell ghosts: sensitivity of angular dependent structure to membrane thickness and refractive index," *Appl. Opt.*, vol. 16, pp. 2036–2038, 1977.

[16] J. C. Lin and A. W. Guy, "A note on the optical scattering characteristics of whole blood," *IEEE Trans. Biomed. Eng.*, vol. 21, pp. 43–45, 1974.

[17] K. S. Yee, "Numerical solution of initial boundary value problem in isotropic media," *IEEE Trans. Antennas Propagat.*, vol. AP-14, pp. 302–307, May 1966.

[18] J. P. Berenger, "A perfectly matched layer for the absorption of electromagnetic waves," *J. Computational Physics*, vol. 114, pp. 185–200, 1994.

[19] P. C. Waterman, "Symmetry, unitarity and geometry in electromagnetic scattering," *Phys. Rev. D*, vol. 3, pp. 825–839, 1971.

[20] P. W. Barber and S. C. Hill, *Light scattering by particles: computational methods.* Singapore: world scientific, 1990.

[21] R. F. Harrington, *Field Computation by Moment Methods*, D. G. Dudley, Ed. IEEE Press, April 1993.

[22] B. T. Drain and Flatau, "Discrete-dipole approximation for scattering calculations," *J. Opt. Soc. Am. A*, vol. 11, pp. 1491–1499, 1994.

[23] B. T. Draine, *Light Scattering by Nonspherical Particles: Theory, Measurements, and Applications*, M. I. Mishchenko, J. W. Hovenier and L. D. Travis, Eds. New York: Academic Press, 2000.

[24] V. I. Tatarski, *Wave propagation in a turbulent medium.* New York: McGraw-Hill, 1961.

[25] A. C. Kak and M. Slaney, *Principles of computerized tomographic imaging.* New York: IEEE Press, 1988.

[26] M. Born and E. Wolf, *Principles of optics.* New York: Pergamon Press, 1959.

[27] http://www.semcad.com/